Surface Plasmon Resonance Imaging of Polymer Microarrays to Study Protein–Polymer Interactions in High Throughput

ARTICLE *in* LANGMUIR · JUNE 2009

Impact Factor: 4.46 · DOI: 10.1021/la900735n · Source: PubMed

3 AUTHORS:

Andrew L Hook
University of Nottingham
54 PUBLICATIONS **941** CITATIONS
SEE PROFILE

Helmut Thissen
The Commonwealth Scientific and Industrial…
134 PUBLICATIONS **2,275** CITATIONS
SEE PROFILE

Nicolas H Voelcker
University of South Australia
420 PUBLICATIONS **5,462** CITATIONS
SEE PROFILE

Langmuir
Article
pubs.acs.org/Langmuir

Surface Plasmon Resonance Imaging of Polymer Microarrays to Study Protein−Polymer Interactions in High Throughput

Andrew L. Hook,[†,‡] Helmut Thissen,[‡,§] and Nicolas H. Voelcker*[,†,§]

[†]*School of Chemistry, Physics and Earth Sciences, Flinders University, Adelaide, 5001, South Australia, Australia,* [‡]*CSIRO Molecular and Health Technologies, Bayview Avenue, Clayton 3168, Victoria, Australia, and* [§]*CSIRO Food Futures Flagship, Riverside Corporate Park, 5 Julius Avenue, North Ryde, 2113, New South Wales, Australia*

Received March 2, 2009. Revised Manuscript Received April 7, 2009

Polymer microarrays provide a high-throughput format in which to assess biointerfacial interactions. This endeavor greatly assists with the development of advanced biomaterials. In order to increase the scope of this platform technology, the development of analytical tools that are compatible with the microarray format and are capable of analyzing biomolecular interactions in high throughput is needed. Here, we show that surface plasmon resonance imaging (SPRi) is such a tool. SPRi enables spatially resolved, surface sensitive, label free, real-time analysis of multiple surface-biomolecular interactions in parallel. In order to demonstrate this, we first printed phenylazide-modified polymers onto a slide coated with a low fouling base polymer. UV irradiation of the slide resulted in the cross-linking of the printed polymer spots to the surface. SPRi was then employed to study the adsorption and desorption of bovine serum albumin, collagen, and fibronectin to these adhesive microarray spots. The spots were also incubated with an adherent cell line, enabling insight into the underlying mechanisms of cell attachment to the polymers studied. For the system analyzed here, electrostatic interactions were shown to dominate cell attachment.

Introduction

Polymer microarrays constitute an emerging key enabling technology for the identification and development of new polymer materials serving specific biomaterial applications. Typically, a polymer microarray consists of an array of different polymers with varying properties in order to assess the biological response, including cell attachment, proliferation, or differentiation to a particular polymer chemistry or topography.[1−3] In one approach to generate a polymer microarray, different ratios of 24 different monomers were arrayed in the presence of an initiator on an epoxy-coated glass substrate.[1] UV irradiation was used to initiate in situ polymerization to form rigid, cross-linked polymer spots. However, only highly cross-linking polymer materials can be assessed by this approach. The resulting types of polymers are poorly defined and might not be easily replicated on a larger scale. Polymer arrays may also be formed by arraying presynthesized polymers on a substrate surface,[3,4] allowing for the analysis of polymer materials fabricated by means of advanced polymerization techniques, such as atom transfer radical polymerization or radical addition−fragmentation chain transfer polymerization.[5,6] Copolymers including block copolymers are also available for printing, further increasing the combinatorial space. Moreover, the polymers can be characterized extensively by conventional techniques before being arrayed. An array of 120 polyurethanes formed by this method was used to identify polymers that promoted the attachment of dendritic cells, which is an important step in the development of phagocytosis assays.[2] This approach has been further developed by incorporating a UV-reactive cross-linker into the polymer arrays, resulting in the formation of covalently surface attached, rigid, stable polymer spots suitable for cell assays conducted over time periods of several days to weeks, during which time polymer spots weakly attached to a surface would normally be susceptible to delamination.[3] Printing of a polymer array in this way on a low-fouling polymer background is particularly beneficial for cell microarrays, as it limits cell attachment to the printed spots.

The high-throughput, expeditious analysis of the resultant polymer microarrays underpins applications of polymer microarrays. Water contact angle measurements, X-ray photoelectron spectroscopy (XPS), and time-of-flight secondary ion mass spectroscopy (Tof-SIMS) measurements have been carried out on a polymer microarray to successfully characterize the properties of each individual spot.[8,9] In the context of cell−material interactions, a range of surface properties must be considered including topography, chemistry, elastic modulus, and charge, with the latter two being difficult to investigate in the microarray format.[4]

Real-time kinetic and thermodynamic analysis of protein binding is useful for the study of biointerfacial interactions and can be used as a first step to deconvolute cell−material interactions. Protein targets are typically fitted with a label, including radioisotopes, fluorophores, enzyme substrates, or haptens. However, the attachment of a label can bring about adverse effects, such as blocking of active epitopes and steric hindrance, as well as altering kinetic properties and affinity constants.[5] Imaging ellipsometry allows the highly sensitive, label-free detection of

*nico.voelcker@flinders.edu.au.

(1) Anderson, D. G.; Levenberg, S.; Langer, R. *Nat. Biotechnol.* **2004**, *22*(7), 863–866.
(2) Mant, A.; Tourniaire, G.; Diaz-Mochon, J. J.; Elliott, T. J.; Williams, A. P.; Bradley, M. *Biomaterials* **2006**, *27*(30), 5299–5306.
(3) Hook, A. L.; Thissen, H.; Voelcker, N. H. *Biomacromolecules* **2009**, *10*(3), 573–579.
(4) Zelzer, M.; Majani, R.; Bradley, J. W.; Rose, F.; Davies, M. C.; Alexander, M. R. *Biomaterials* **2008**, *29*(2), 172–184.
(5) Seidel, M.; Niessner, R. *Anal. Bioanal. Chem.* **2008**, *391*(5), 1521–1544.
(6) Asinovski, L.; Beaglehole, D.; Clarkson, M. T. *Phys. Status Solidi A* **2008**, *205*(4), 764–771.
(7) Yeatman, E.; Ash, E. A. *Electron. Lett.* **1987**, *23*(20), 1091–1092.
(8) Smith, E. A.; Corn, R. M. *Appl. Spectrosc.* **2003**, *57*(11), 320A–332A.
(9) Steiner, G. *Anal. Bioanal. Chem.* **2004**, *379*(3), 328–331.

surface-binding events with high spatial resolution; however, incorporation of a flowthrough system for real-time analysis is not currently possible.[6] Surface plasmon resonance imaging (SPRi), in comparison, enables spatially resolved, surface-sensitive, label-free, real-time analysis of surface−biomolecule interactions and is compatible with the microarray format. Typically, the reflected light from an SPR experiment is detected by a camera or viewed through a microscope, enabling spatial measurements of changes in the thickness or refractive index at a particular surface.[7] This feature of SPRi permits the label-free, rapid, and parallel analysis of the adsorption of a particular biomolecule to an array of sample spots under identical environmental conditions. The lateral resolution of SPRi is limited by the propagation length of the excited surface plasmons, which is dependent on the dielectric constant of the metal film (ε_m), the refractive index of the dielectric (η_s), and the frequency of the incident light (w_0).[8] Under optimized conditions, a resolution of less than 2 μm can be achieved.[9] Formation of chemically or biologically patterned surfaces by microfluidics, robotic spotting, and lithographic approaches has been utilized for the observation of spatially directed bimolecular adsorption by SPRi.[14,16−18] SPRi has been employed to monitor biointerfacial interactions including DNA hybridization,[10] protein−material interactions,[11] protein−DNA interactions,[12] avidin−biotin binding,[13] protein−carbohydrate interactions,[14] antibody−antigen interactions,[15] and small molecule−protein interactions.[16] However, the surface patterning in these studies resulted in homogeneous surface coatings with comparable refractive index. In order to enable the simultaneous surface plasmon resonance (SPR) analysis of a diverse polymer library (presented as a microarray) containing distinctly different polymer chemistries with a broad range of dielectric properties, densities, and 3D structures, careful considerations must be given to adequate procedures that allow quantitative comparisons of SPR measurements on these diverse spots.[16]

In the present study, three polymers with disparate chemistries were investigated for their interaction with biomolecules of interest. These polymers were arrayed using a robotic spotting device, which is readily available to life science laboratories interested in cell−material interactions. Since the printed polymer spots on the array invariably present thickness, density, and refractive index variations, we have devised a method to comparably and simultaneously conduct SPR measurements on a polymer microarray. This approach was used to investigate the kinetics and thermodynamics of bovine serum albumin (BSA), fibronectin (FN), and collagen (CN) type I adsorption on the polymer microarray spots. In addition, cell attachment to the polymer spots was also investigated.

Experimental Section

Substrate Preparation. SPR chips (SPR-1000-050, GWC Technologies) with a gold coating of 45 nm on glass (Schott, SF10) were used as received.

Poly(ethylene glycol) (PEG) coatings were prepared as previously described.[17] Initially, SPR chips or glass slides were coated by plasma polymerization of allylamine in a custom-built reactor described elsewhere.[18] In short, the plasma reactor consisted of two circular electrodes separated by 12.5 cm in a cylindrical reactor being 35 cm high with a diameter of 17 cm. Allylamine (Aldrich, 98% purity) was used as a monomer. Allylamine plasma polymer (ALAPP) deposition occurred at a frequency of 200 kHz, a power of 20 W, and an initial monomer pressure of 0.200 mbar. The deposition time was 5 s. Freshly deposited ALAPP samples were left overnight in hexamethylene diisocyanate (HDI) at room temperature in the absence of water. Subsequently, samples were washed thrice for 10 min in acetonitrile (Merck, 99.9% purity). HDI-modified samples were incubated overnight at 45 °C in a solution of hydroxyl-terminated star-PEG (MW 116 000, 24 arms, Shearwater Polymers, USA) in acetonitrile (3 mg/mL). Subsequently, samples were washed in Milli-Q water (18.2 MΩ. cm) thrice for 1 h and finally air-dried.

Array Formation. Poly(acrylic acid) (PAA) (Aldrich, MW 90 000, η = 1.527), poly(ethylene imine) (PEI) (MW 70 000, η = 1.48), and poly(L-lysine) (PLL) (Sigma, MW 70 000, η = 1.37) were spotted onto either the SPR chips or on the PEG-coated SPR chips. Arrays for cell growth studies were spotted onto PEG-coated glass slides.

Before spotting, polymer samples were prepared at 4, 2, 1, 0.5, 0.25, 0.1, 0.05, and 0.01 mg/mL concentrations in Milli-Q water. A solution of Milli-Q water was also spotted as a negative control. For formation of covalently cross-linked PEI and PLL polymer spots ((PEI-c) and (PLL-c), respectively), PEI and PLL were spotted onto PEG-modified SPR chips. Before spotting, polymer samples were prepared at 0.5 mg/mL solutions in Milli-Q water containing 1.0 mg/mL (3.3 mM) *N*-succinimidyl-5-azido-2-nitrobenzoate (NSANB) (Fluka). Polymer-NSANB solutions were incubated at 25 °C for 10 min before spotting commenced. For the formation of covalently cross-linked PAA spots (PAA-c), PAA (4.0 mg/mL) was prepared in Milli-Q water (50 μL) containing 75 mM *N*-hydroxysuccinimide (NHS) (Sigma) and 30 mM 1-ethyl-3-(3-dimethylaminopropyl)carbodiimide hydrochloride (EDC) (Fluka) and incubated for 1 h at 37 °C. 50 μL of 2.00 mg/mL (6.6 mM) NSANB in Milli-Q water containing 7.0 mM ethylenediamine (Merck) at 25 °C was incubated for 10 min before addition of the 50 μL activated PAA, to make a final volume of 100 μL, and incubated for a further 10 min before spotting commenced. Polymers were arrayed using a BioOdyssey Calligrapher MiniArrayer (Bio-Rad) with a 375 μm diameter circular, solid pin (ArrayIt) delivering approximately 4.0 nL/spot. After array formation, samples were exposed to UV irradiation (25 W) for at least 10 min, which was sufficient time to ensure cross-linking.[3] The UV lamp (multiband source, 254−365 nm) was held at a distance of 1 cm from the sample.

PAA-c samples were also treated with CN type I (from rat tail, Sigma). Here, a 335 μm width square, solid pin was used. After array formation and cross-linking, a PAA-c array was incubated with 50 μg/mL CN solution in 0.05 M phosphate buffer for 2 h at 25 °C before the CN solution was removed using a pipet. One millimolar acetic acid was added in the initial formation of the CN solution to assist with the dissolution of CN type I.

Profilometry. The thickness and profile of the arrayed spots was determined by profilometry using a Dektak 6 M Stylus Profiler (Veeco). A diamond stylus of radius 12.5 μm was moved over the surface at a resolution of 0.25 μm per data point and a stylus force of 5 mg. Each spot was measure thrice. The rims of spots were ignored for height measurements.

SPR Imaging. SPRi was conducted using a SPRimagerII (GWC Technologies Inc.). A collimated polychromatic *p*-polarized light source was impinged onto a gold film sample through a prism assembly at an angle of incidence (θ) to excite surface

(10) Bassil, N.; Maillart, E.; Canva, M.; Levy, Y.; Millot, M. C.; Pissard, S.; Narwa, W.; Goossens, M. *Sens. Actuators B* **2003**, *94*(3), 313–323.
(11) Jordan, C. E.; Corn, R. M. *Anal. Chem.* **1997**, *69*(7), 1449–1456.
(12) Brockman, J. M.; Frutos, A. G.; Corn, R. M. *J. Am. Chem. Soc.* **1999**, *121* (35), 8044–8051.
(13) Jordan, C. E.; Frutos, A. G.; Thiel, A. J.; Corn, R. M. *Anal. Chem.* **1997**, *69* (24), 4939–4947.
(14) Smith, E. A.; Thomas, W. D.; Kiessling, L. L.; Corn, R. M. *J. Am. Chem. Soc.* **2003**, *125*(20), 6140–6148.
(15) Kyo, M.; Usui-Aoki, K.; Koga, H. *Anal. Chem.* **2005**, *77*(22), 7115–7121.
(16) Kanoh, N.; Kyo, M.; Inamori, K.; Ando, A.; Asami, A.; Nakao, A.; Osada, H. *Anal. Chem.* **2006**, *78*(7), 2226–2230.
(17) Thissen, H.; Johnson, G.; McFarland, G.; Verbiest, B. C. H.; Gengenbach, T. R.; Voelcker, N. *Proc. SPIE* **2006**, *6413*(64130B), 1–9.
(18) Griesser, H. J. *Vacuum* **1989**, *39*(5), 485–488.
(19) Green, R. J.; Frazier, R. A.; Shakesheff, K. M.; Davies, M. C.; Roberts, C. J.; Tendler, S. J. B. *Biomaterials* **2000**, *21*(18), 1823–1835.

plasmons, which results in a loss of energy from the incident beam and a decrease in the intensity of the reflected light.[19] The excitation of surface plasmons is maximized at a specific resonance angle θ_r. The Kretschmann configuration was adopted in order to satisfy momentum matching conditions that are not met when light illuminates a planar metal/dielectric interface.[20] The light reflected from the sample passed through a narrow band-pass filter (800 nm) and was detected by a charge coupled detector (CCD) camera, which was able to capture an image of the entire optical field of the chip surface. Images were analyzed using V++ Precision Digital Imaging System (V.4).

SPR signal standardization studies were conducted by initially forming a polymer array onto a gold-coated SPR chip made out of glass. The surface was initially washed with 0.05 M phosphate buffer (Na_2HPO_4, 1.41 g/L; KH_2PO_4, 0.24 g/L) at a flow rate of 3 μL/s. The SPR signal for each spot was then measured against the angle of incidence of the impinging light beam and an optimal angle for subsequent fixed angle SPR measurements was selected, whereupon, for a plot of reflectivity against angle of incidence the absolute value of the differential reflectivity is maximized. This was typically at an angle slightly lower than the resonance angle. The intensity of the reflected light was monitored. 0.1% (v/v) ethanol in water was then injected over the array until equilibrium was reached at a flow rate of 3 μL/s. The SPR signal for each spot was then again measured against the angle of incidence of the impinging light beam. This allowed for the measurement of the shift in the resonance angle as a result of a change in the bulk refractive index of the buffer.

All biomolecular adsorption measurements were taken over an angle of incidence range of 48−57° while the temperature was held constant at 25 °C. Initially, the polymer microarray was primed in 0.05 M phosphate buffer at pH 7.4. Once a stable background was reached, the SPR signal for each spot was measured against the angle of incidence of the impinging light beam. Then protein solutions of 10 μg/mL, 5 μg/mL, 2 μg/mL, or 1 μg/mL were injected until SPR signal reached a plateau. Here, we used albumin (from bovine serum, Sigma), FN (from bovine plasma, Sigma) and CN type I (from rat tail, Sigma). The flow rate of 5 μL/s was used to ensure that kinetic measurements were not limited by mass transport of the adsorbant from the bulk solution. One millimolar acetic acid added to assist with the dissolution of CN type I, reduced the pH from 7.4 to 7.35, while BSA and FN were dissolved in phosphate buffer with a pH of 7.4. The surface was then washed with 0.05 M phosphate buffer at 5 μL/s to allow desorption of weakly bound biomolecules, before the SPR signal for each spot was once again measured against the angle of incidence of the impinging light beam. The surface was subsequently regenerated by washing with 0.1% Tween solution at a flow rate of 3 μL/s for 60 s and, based upon the isoelectric point of the protein being used, 0.1 M NaOH solution at a rate of 3 μL/s for 60 s or 0.1 M HCl solution at a rate of 3 μL/s for 60 s in order to switch the net charge of the adsorbed biomolecules. The surface was then washed with 0.05 M phosphate buffer at a flow rate of 3 μL/s until baseline was again reached.

SPR signal intensity versus angle of incidence curves measured for varied polymer spots before and after biomolecular interaction events were modeled using Winspall V 3.01 software,[21] which applies the Fresnel equations for a n-layered system where n can be varied.[22] Simulation parameters used were a 60° triangular prism using p-polarized light of 800 nm wavelength. Refractive index values used were SF10 glass $\eta = 1.71129$, gold $\eta = 0.16 + 4.84i$,[23,24] biopolymer layer $\eta = 1.45$[25] and water $\eta = 1.329\,08$.[26] For curve fitting, only the position of the resonance angle was considered.

Cell Growth. A SK-N-SH neuroblastoma cell line was used for cell attachment experiments. Cells were cultured in Dulbecco's modified eagle media (DMEM) containing penicillin and streptomycin and incubated at 37 °C, 5% CO_2, and 60−70% humidity. SK-N-SH cells were seeded onto surfaces at a seeding density of 5×10^4 cells/cm^2 and allowed to attach to the surface after which they were incubated at 37 °C, 5% CO_2, and 60−70% humidity for 24 h. Cells were then stained with Hoechst 33342 dye (10 μg/mL) for a further 5 min before analysis by fluorescence microscopy. Cells were visualized with an IX81 Olympus fluorescence microscope and analyzed using analySIS LS Research v2.5 software using a 360−370 nm excitation filter and a 420 nm suppression filter to detect Hoechst 33342 fluorescence. Captured images were modified using Adobe Photoshop software.

Kinetic Analysis. A complete description of the kinetic analysis is provided in the Supporting Information. In short, the association constant (k_a), the dissociation constant (k_d), and the binding constant (K) was determined by assuming a first-order kinetic process whereupon the protein in bulk solution adsorbs to a surface binding site resulting in a measurable concentration of protein at the surface (Γ_s).

The surface concentration of the adsorbed species at saturation ($\Gamma_{s\infty}$) was determined by assuming Langmuir binding between protein and the surface.

Results and Discussion

Standardizing SPR Signal on a Polymer Microarray for Biomolecule Adsorption. PLL was arrayed onto bare SPR gold chips from a concentration series ranging from 0 to 2 mg/mL. A surface plot of the resultant SPR signal intensity obtained of the array formed from such a concentration series is shown as Figure 1. The angle of incidence was set such that the bare gold background was in resonance (appeared dark). For the polymer array formed in Figure 1, the polymer spots range in thickness from 0 to 54 nm as determined by profilometry. At a given angle, this results in differences in the attenuation of a light beam impinging upon the surface as compared with the uncoated regions, which allows each spot to be spatially resolved by SPR imaging. The intensity of the reflected light is enhanced at the PLL spots from the higher concentrations due to the displacement of the resonance angle to higher angles as a result of the local increase in the refractive index. For thicker spots formed from higher polymer concentrations, the shift in resonance angle is greater resulting in a larger increase in reflectivity.

A fixed angle SPR adsorption experiment is typically conducted at an angle at which the greatest absolute value of the differential of SPR reflectivity occurs for the surface being studied in order to gain the highest sensitivity.[25] This angle is obtained from a plot of reflectivity against angle of incidence, which will vary for a polymer array featuring spots of varied thickness or refractive index. Therefore, the change in reflectivity measured at each spot at a fixed angle may be different upon adsorption of the same amount of biomolecular species. Thus, in order to measure biomolecular adsorption events on a polymer microarray it is advantageous to measure the shifts in resonance angle occurring at each spot as opposed to monitoring changes in reflectivity.

If on the other hand one desires to obtain real-time kinetic measurements by SPRi, fixed angle experiments are inevitable since the current SPRi instrumentation does not allow fast enough angle changes. However, knowing the relationship between the reflectivity against angle of incidence for a particular spot, one can measure the change in reflectivity (ΔR) upon biomolecular

(20) Kretschmann, E. *Z. Phys. A: Hadrons Nucl.* **1971**, *241*(4), 313–324.
(21) http://www.mpip-mainz.mpg.de/knoll/soft/index.html. In.
(22) Heaven, O. S. *Optical properties of thin solid films*; Dover: New York, 1965.
(23) Schulz, L. G. *J. Opt. Soc. Am.* **1954**, *44*(5), 357–362.
(24) Schulz, L. G.; Tangherlini, F. R. *J. Opt. Soc. Am.* **1954**, *44*(5), 362–368.
(25) Brockman, J. M.; Nelson, B. P.; Corn, R. M. *Annu. Rev. Phys. Chem.* **2000**, *51*, 41–63.
(26) Schiebener, P.; Straub, J.; Sengers, J.; Gallagher, J. S. *J. Phys. Chem. Ref. Data* **1990**, *19*,(3), 677–717.

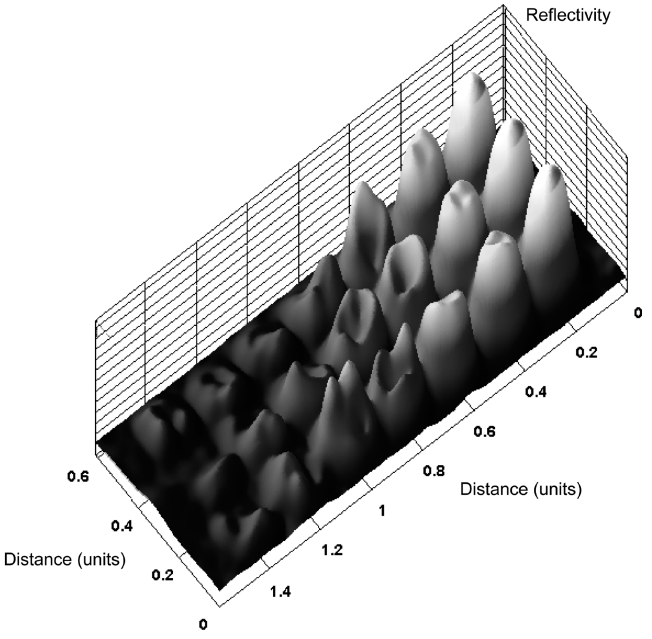

Figure 1. Surface plot of reflectivity taken from an array of PLL spotted onto a SPR gold chip over a concentration series of 2.0, 1.0, 0.5, 0.25, 0.1, 0.05, and 0.01 mg/mL. Each concentration was spotted in triplicate. Each spot was approximately 400 μm in diameter, with a center-to-center distance of 500 μm.

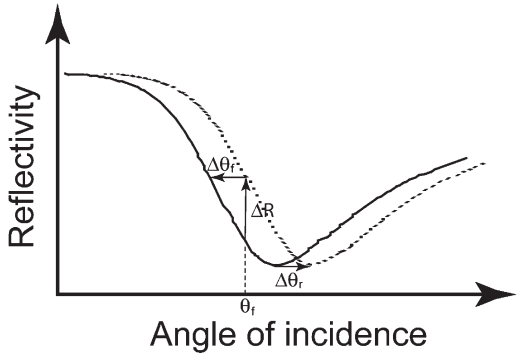

Figure 2. Schematic depicting the method used to convert a measured change in reflectivity to the shift in the resonance angle. On a given SPR chip surface, an adsorption event results in a shift in the reflectivity versus angle of incidence curve from the solid to the dotted curve. $\Delta\theta_r$ is the change in the resonance angle. At an angle of incidence θ_f used for a fixed angle experiment, the change in reflectivity upon adsorption corresponds to ΔR. The corresponding resonance angle shift $\Delta\theta_f$ is assumed to be equal to $\Delta\theta_r$.

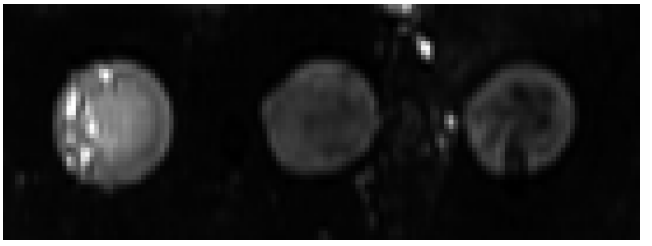

Figure 3. SPR image of a section of an array of PAA spotted at initial polymer concentrations of 1.0, 0.5, and 0.25 mg/mL. The center-to-center distance between spots is 750 μm, and the spot diameter is approximately 430 μm from a 375 μm diameter solid pin.

adsorption in real time at a judiciously chosen fixed angle (θ_f), being an angle where a shift in the resonance angle produces an optimized shift in reflectivity for all regions on the surface, and convert those changes into a shift in the resonance angle ($\Delta\theta_f$) using the relationship between the resonance angle and reflectivity that can be measured immediately before biomolecular adsorption commences, as depicted in Figure 2. Using this approach, every change in reflectivity measured during a fixed angle experiment can be converted to the corresponding shift in resonance angle ($\Delta\theta_r$), based upon the assumption that $\Delta\theta_f = \Delta\theta_r$.

As a proof of principle, a PAA array spotted from polymer solutions with a concentration of 1.0, 0.5, and 0.25 mg/mL onto a bare gold SPR chip was prepared. An SPR image of a part of the array is shown in Figure 3. After a stabilizing phase in phosphate buffer for 1000 s, the average reflectivity and the change of reflectivity versus angle of incidence over the entirety of each of the spots as well as the unmodified bare gold background were measured as shown in Figure 4.

The resonance angle on the PAA spots was higher than for unmodified gold (50.4°, 50.2°, and 50.1° for polymer concentrations of 2.0 mg/mL, 1.0 mg/mL, 0.5 mg/mL, respectively, compared to 49.8° for uncoated gold) (Figure 4A). The greatest differentials of the reflectivity were found in the range 48.9−49.4° (Figure 4B). An angle of 48.9° was hence selected for subsequent fixed angle measurements.

A solution of 1% ethanol in water was injected into the SPR flow cell holding the PAA array at 3 μL/s and the SPR signal intensity was measured over time (Figure 5A). The exchange of fluid medium is expected to result in a change in refractive index that is consistent across the entire surface, thus leading to the same SPR angle shift at each spot. A decrease in the reflectivity was observed (Figure 5A) corresponding to a negative shift in the resonance angle. Notably, however, the change in reflectivity was significantly different for the different spots, ranging from −13 to −27 units. Clearly, thickness differences between spots printed at different concentrations prevent measuring a constant change in reflectivity upon exposure to a medium with a different bulk refractive index.

Reflectivity versus angle of incidence curves were measured before and after fluid medium change (Figure 5C), at time periods 0 and 3000 s allowing the determination of $\Delta\theta_r$. Using the curve taken before the fluid medium change, the corresponding shift in the resonance angle can be found for every change in reflectivity measured at θ_f, as described in Figure 2. For this calculation, the assumption that $\Delta\theta_f = \Delta\theta_r$ must be validated. In order to achieve this, the measured shift in the resonance angle at varied θ_f was determined from the reflectivity versus angle of incidence curves taken before and after the fluid medium change, shown in Figure 5C. The resultant $\Delta\theta_f$ values are shown as Figure 6. From this curve, it can be seen that for uncoated gold and the PAA array spotted at 0.5 mg/mL $\Delta\theta_f = \Delta\theta_r$ over most angles below the θ_r except at very low θ_f ($< 48.5°$). However, for the PAA array spotted at 1.0 and 2.0 mg/mL the $\Delta\theta_f$ measured initially decreased from approximately −0.10° to −0.16° as the θ_f was increased from 48.5° to 49.5°. At a θ_f above 49.5°, the measured $\Delta\theta_f$ values gradually increased from −0.16° to the measured $\Delta\theta_r$ of −0.147°. Thus, in order to make the total measured $\Delta\theta_f$ comparable over all spots, irrespective of their thickness or refractive index, measurements were standardized by the total $\Delta\theta_r$ measured for each spot. The resultant kinetic curves showing changes in resonance angle are shown in Figure 5B, and here all four spots measure similar resonance angle shifts with an average value of −0.147°. As determined by SPR measurements, the phosphate buffer solution used has a $\eta = 1.3355$. A 1% ethanol solution has a refractive index of 1.3336; thus, the change in refractive index was 0.0019. This should correspond to a

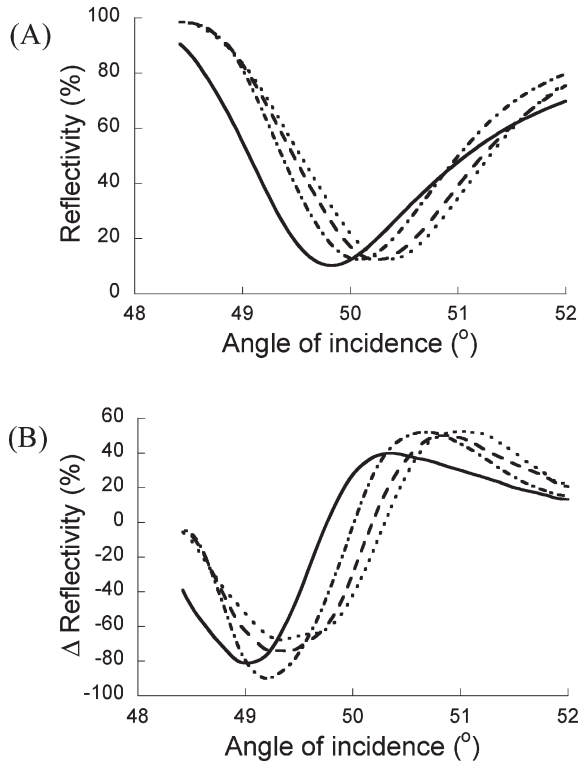

Figure 4. (A) Reflectivity (%) and (B) reflectivity (%) versus angle of incidence spectra for PAA spotted change in at (dotted line) 2.0 mg/mL, (dashed line) 1.0 mg/mL, (dot−dashed line) 0.5 mg/mL, and (solid line) uncoated gold in phosphate buffer.

resonance angle shift of −0.141° as determined by modeling this buffer exchange using Winspall software. This value is very close to the experimentally determined value of −0.147°, well within the limits of the experimental error, validating our approach. We hence conclude that our system of standardizing reflectivity data is capable of comparing changes in refractive index occurring at spots with different thicknesses or dielectric properties and that it can therefore be employed for the analysis of biomolecular interactions on a polymer microarray.

Kinetic Analysis of Protein Adsorption to Polymer Microarray. The adsorption of BSA, a globular serum protein present in cell culture media, FN, a globular extracellular matrix (ECM) protein that is important for cell attachment and contains the RGD cell adhesion mediating sequence, and CN type I, which is a protein also integral to the ECM and involved largely with the structural properties of the ECM, to a polymer microarray was studied by SPRi. These proteins were selected for proof-of-principle purposes but also because of the important role of these proteins in mediating cell adhesion. For these studies, a polymer microarray was first deposited on a HDI-PEG layer. A thin ALAPP layer was deposited and incubated overnight with HDI. This step activated the layer for subsequent grafting of a hydroxyl-terminated star-PEG layer with low fouling properties.[17] This approach has advantages over the use of a PEGylated alkanethiol,[27] since it can be used to coat almost any material of choice including glass or silicon, which allows this coating to be readily transferred from a SPR chip to a substrate for cell attachment and outgrowth assays. Thus, this approach provides a favorable alternative to self-assembled monolayers of thiols or the use of dextran for coating SPR chips.

After the HDI-PEG layer had been deposited, a resonance angle shift of 1.14° was measured corresponding to a thickness of 10.6 nm assuming the layer has a refractive index of 1.5,[28] as determined by Winspall curve fitting software. Initially, a polymer array of PAA-c, PEI-c, and PLL-c was formed on the PEG-coated substrate utilizing the photo-cross-linking methodology reported previously.[3] Functionalization of the polymers with NSANB, which introduces a photoresponsive phenylazide group, allowed for the surface immobilization and random intra- and intermolecular cross-linking of the polymer spots and the covalent binding to the underlying substrate upon UV irradiation. Polymers were spotted at concentrations above 0.25 mg/mL to ensure complete coverage. Both PEI and PLL were spotted at 0.5 mg/mL, while PAA was spotted at 2.0 mg/mL. A higher spotting concentration was chosen for PAA, since these polymers could not be successfully transferred at a lower concentration of 0.5 mg/mL. A typical SPRi image of representative polymer spots is shown in Figure 7A. The proportional increase of the polymer thickness with the resultant shift in SPR angle enables one parameter to be determined from the other. For the polymer array used, the average thicknesses for PAA-c, PEI-c, and PLL-c were 2.2, 8.3, and 18.8 nm, respectively, as determined from the reflectivity versus angle of incidence curves shown as Figure 7B and Winspall curve fitting software, which is based upon Fresnel equations.[22] These results correspond well with the spot thicknesses measured by means of profilometry in the dry state, which gave values of 1.4, 18.3, and 21.3 nm for PAA-c, PEI-c, and PLL-c, respectively. Differences between values obtained from SPRi and profilometry could arise from differences between the wet and dry state of the polymers and varied humidity and temperature during printing. As thickness values determined from both profilometry and from modeling shifts in resonance angle using Winspall software were in reasonable agreement, all subsequent thickness measurements were taken by modeling resonance angle shifts with Winspall software.

This polymer array was investigated for the adsorption and desorption of FN, CN type I, and BSA at various solution concentrations. Kinetic plots for the adsorption of CN type I, FN, and BSA to the polymer array are shown in Supporting Information Figures SI1−3. A representative kinetic plot is shown in Figure 8. In order for $\Gamma_{s\infty}$ to be quantitatively comparable, the measured changes in reflectivity were converted to resonance angle shifts as previously explained. Thus, reflectivity versus the angle of incidence was measured for each spot at time point 0 s and once the biomolecular desorption had plateaued. The shift in resonance angle from each spot was converted to an increase in thickness by modeling using the Winspall program, assuming a refractive index of this layer of 1.45. Assuming a monolayer coverage with a density of 1.35 g/cm,[3,29] the biomolecular thickness was converted into Γ_s with units of mg/m^2.

Adsorption curves at varied protein concentration were analyzed assuming a first-order kinetic process. However, this model is simplistic for a protein adsorption process, which may include complex processes such as protein−surface interactions, changes in protein conformation, reorientation of proteins, and surface diffusion.[30] Nevertheless, plots of $d\Gamma_s/dt$ against Γ_s produced a linear curve with high R^2 values, as shown for each biomolecular adsorption reaction in Supporting Information Table SI1, with

(27) Holmlin, R. E.; Chen, X. X.; Chapman, R. G.; Takayama, S.; Whitesides, G. M. *Langmuir* **2001**, *17*(9), 2841–2850.

(28) Zhang, Z.; Knoll, W.; Foerch, R. *Surf. Coat. Technol.* **2005**, *200*(1−4), 993–995.

(29) Fischer, H.; Polikarpov, I.; Craievich, A. F. *Protein Sci.* **2004**, *13*(10), 2825–2828.

(30) Silin, V.; Weetall, H.; Vanderah, D. J. *J. Colloid Interface Sci.* **1997**, *185*(1), 94–103.

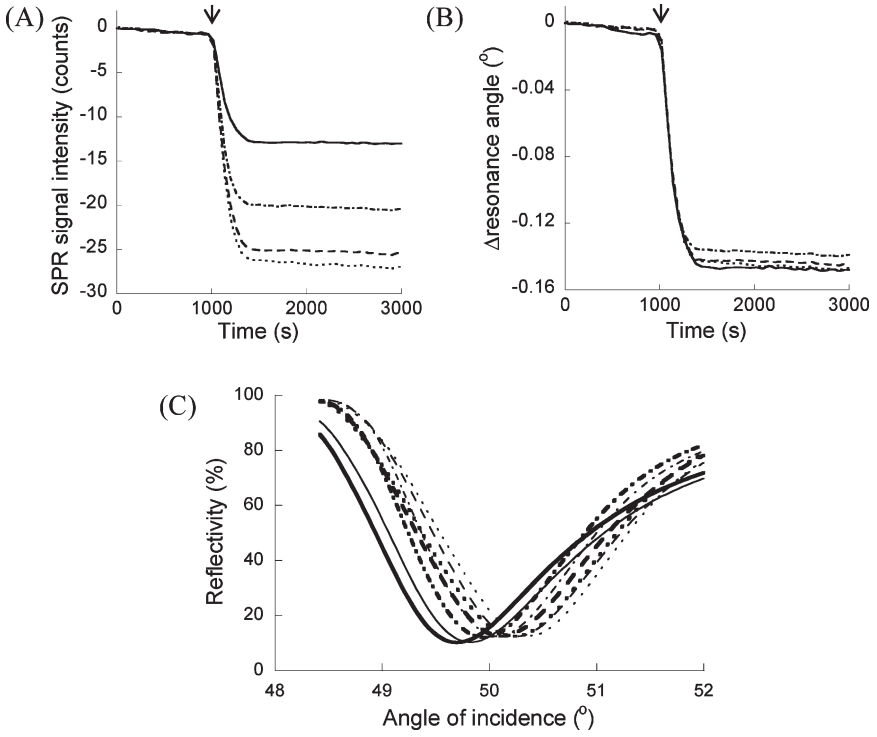

Figure 5. SPRi measurements of a PAA array spotted at (dotted line) 2.0 mg/mL, (dashed line) 1.0 mg/mL, (dot−dashed line) 0.5 mg/mL, and (solid line) uncoated. The measurements started in phosphate buffer and after 1000 s (as indicated by the arrows), 1% ethanol in water was added. (A) SPR sensorgram showing reflectivity data for each spot; (B) SPR sensorgram showing resultant Δ resonance angle data after converting the measured change in reflectivity from (A) with the measured shift in the resonance angle in (C); (C) reflectivity (%) versus angle of incidence spectra for PAA spots before (thin) and after (bold) the addition of 1% ethanol solution.

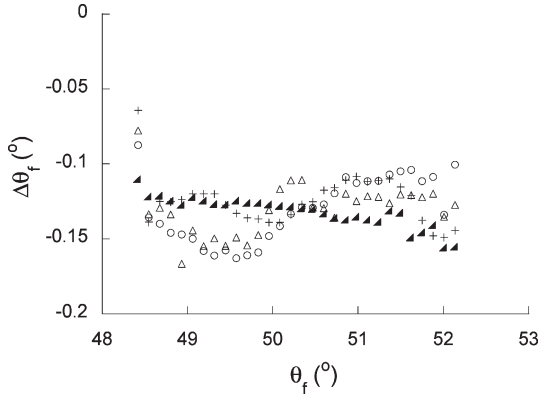

Figure 6. The shift in resonance angle measured between the curves shown in Figure 5C, taken before and after the addition of 1% ethanol, from different angles of incidence along the initial reflectivity versus angle of incidence curve for a PAA array spotted at (○) 2.0 mg/mL (θ_r = 50.4°), (△) 1.0 mg/mL (θ_r = 50.2°), (+) 0.5 mg/mL (θ_r = 50.1°), and (solid right angle triangle) uncoated (θ_r = 49.8°).

values typically of >0.97, except when low (<0.1 nm) or no Γ_s was measured such as when 1 μg/mL protein concentrations were used. This suggests that a first-order protein adsorption process dominates kinetics over the initial time period; thus, this (admittedly simplified) model was used to analyze the kinetic data further. The resultant k_a, k_d, K, and $\Gamma_{s\infty}$ for each polymer with each adsorbed protein is shown in Table 1. The dimensions of CN type I, FN, and BSA are a length of 300 nm and a diameter of 1.5 nm,[31] a length of 15.5 nm and a diameter of 8.8 nm,[32] and a length of 14.0 nm and a diameter of 4.0 nm,[33] respectively. The maximum theoretical monolayer coverage for side-on ($\Gamma_{side\text{-}on}$) and end-on ($\Gamma_{end\text{-}on}$) orientations were determined as described in the Supporting Information. The $\Gamma_{side\text{-}on}$ and $\Gamma_{end\text{-}on}$ determined for CN type I, FN, and BSA adsorption onto the polymer array are shown in Supporting Information Table SI2.

A CN type I layer of average thickness of approximately 4 nm was observed to deposit on the PAA-c after approximately 2000 s at a solution concentration of 10 μg/mL (Supporting Information Figure SI1A); however, almost no adsorption was observed on the PEI-c and PLL-c polymers (Supporting Information Figure SI1B−C). This was reflected in the high k_a, K, and $\Gamma_{s\infty}$ of 102.4×10^3 s^{-1} M^{-1}, 2555.5×10^6 M^{-1}, and 15.7 mg/m^2, respectively, and the low k_d value of 0.401×10^{-4} s^{-1} calculated for CN type I adsorption to PAA-c as compared with PEI-c and PLL-c. (Table 1). The $\Gamma_{s\infty}$ of CN type I to PAA-c of 15.7 mg/m^2 is higher than the $\Gamma_{side\text{-}on}$ of 1.5 mg/m^2 but lower than the $\Gamma_{end\text{-}on}$ of 283.2 mg/m^2 for CN type I adsorption (Supporting Information Table SI2). This suggests that CN type I adsorbs to PAA with part of the protein lying flat on the surface while other regions adopt an end-on orientation.

In the case of FN, the adsorbed layer thickness on PAA-c averaged 1.0 nm after adsorption for 1500 s at 10 μg/mL FN solution concentration (Supporting Information Figure SI2A), and lower thickness values of 0.5 and 0.2 nm were obtained on PEI-c and PLL-c, respectively (Supporting Information Figure SI2B and C). Interestingly, FN adsorption to PAA-c had a higher k_a than to both PEI-c and PLL-c despite both the latter polymers being positively charged. The $\Gamma_{s\infty}$ for FN adsorption to

(31) Dupont-Gillain, C. C.; Jacquemart, I.; Rouxhet, P. G. *Colloids Surf., B* **2005**, *43*(3−4), 179–186.
(32) Koteliansky, V. E.; Glukhova, A. A.; Bejanian, M. V.; Smirnov, V. N.; Filimonov, V. V.; Zalite, O. M.; Venyaminov, S. Y. *Eur. J. Biochem.* **1981**, *119*(3), 619–624.
(33) Zhang, M. Q.; Desai, T.; Ferrari, M. *Biomaterials* **1998**, *19*(10), 953–960.

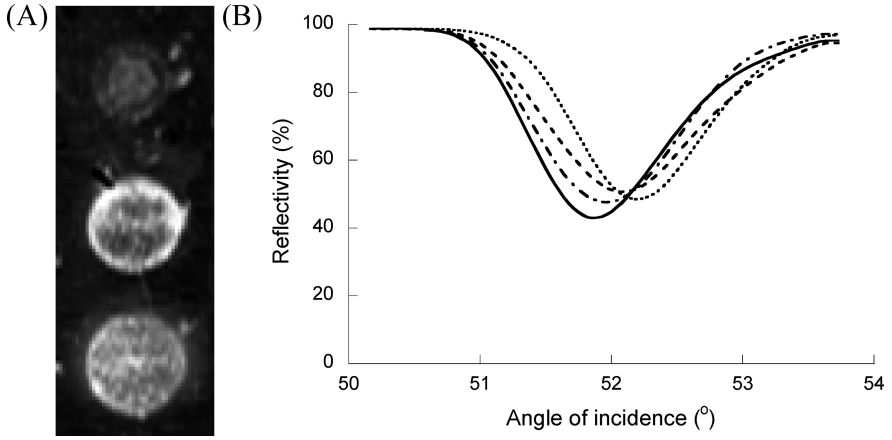

Figure 7. (A) SPR image of representative polymer spots. From top to bottom, spots correspond to PAA-c, PEI-c, and PLL-c. Spot diameter is approximately 400 μm; (B) Reflectivity (%) versus angle of incidence spectra for (dot−dashed line) PAA-c, (dotted line) PEI-c, and (dashed line) PLL-c on (solid line) HDI-PEG coating.

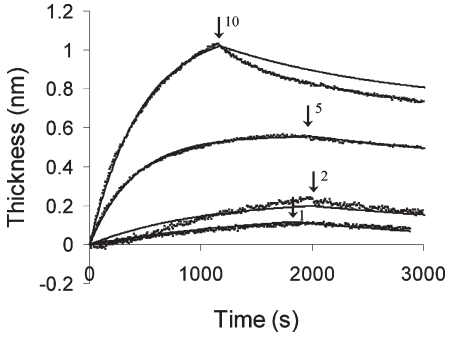

Figure 8. SPR sensorgrams, showing both the experimental data (dots) and fitted curves according to the constants shown in Table 1 (solid line), for the adsorption and desorption of FN, at concentrations of 10 μg/mL, 5 μg/mL, 2 μg/mL, and 1 μg/mL at pH 7.4, to PAA-c. All curves have had the background subtracted (change in thickness measured for the unmodified HDI-PEG coating). Protein was injected once the surface had stabilized in phosphate buffer. Protein injection occurred at 0 s. Phosphate buffer was injected as indicated by the arrows. The number next to the arrow indicates which FN concentration it is referring to.

PAA-c, PEI-c, and PLL-c, found to be 15.3, 3.2, and 0.5 mg/m^2, respectively (Table 1), compared with the $\Gamma_{\text{side-on}}$ of 5.5 mg/m^2 and the $\Gamma_{\text{end-on}}$ of 9.1 mg/m^2 (Supporting Information Table SI2) suggests that FN adsorbed to PEI-c and PLL-c in a side-on orientation, whereas FN adsorbed to PAA-c in a end-on orientation, possibly forming interdigitated or multilayers . The $\Gamma_{s\infty}$ determined for FN adsorption to Au, Ti-oxide, and Ta-oxide of 14.6, 10.6, and 11.0 mg/m^2 [34] are comparable with the FN adsorption measured to PAA-c, also above the theoretically determined $\Gamma_{\text{end-on}}$. Significantly,the pK_a of both PAA and Ta-oxide are approximately 3, thus would both have a similar negative charge.[42,43]

BSA adsorption was observed on both PEI-c and PLL-c, with adsorption for 1500 s at 10 μg/mL resulting in surface-bound protein layers of 0.4 and 0.2 nm thickness, respectively (Supporting Information Figure SI3B and C). Conversely, little to no BSA adsorption was measurable on the PAA-c (Supporting Information Figure SI3A). In fact, a negative change in thickness was measured for PAA-c (Supporting Information Figure SI3A). Since the SPR sensorgrams shown in Supporting Information Figures SI1−SI3 have had the signal from the unmodified HDI-PEG background subtracted, this negative result is likely due to the PAA-c resisting BSA adsorption more effectively than the PEG background. BSA has an isoelectric point (pI) of 4.7[35] and is, thus, negatively charged at physiological pH. The resistance of BSA adsorption by PAA-c is therefore likely to be due to the electrostatic repulsion of the overall negative charge of the protein with the negative charge of PAA. Likewise, the adsorption to PEI-c and PLL-c is likely due to electrostatic attraction between the overall negative charge of BSA and the positive charge of PEI and PLL. Adsorption of BSA has previously been shown to be electrostatically mediated.[38,45] The $\Gamma_{s\infty}$ of BSA adsorption to PEI-c and PLL-c is higher than the determined $\Gamma_{\text{side-on}}$ of 2.0 mg/m^2 for BSA adsorption but lower than the $\Gamma_{\text{end-on}}$ of 6.7 mg/m^2 (Supporting Information Table SI2), suggesting that the adsorbed BSA has an orientation between a side-on and an end-on orientation. BSA adsorption to PLL has previously been studied giving a Γ_s of 6.5 mg/m^2.[36] This higher BSA adsorption is likely due to the lower pH of 5 at which the adsorption was conducted in that study. The low adsorption of BSA to PAA, which was found to be lower than the BSA adsorption onto the HDI-PEG background, inhibited further analysis in this case.

The detailed discussion of protein polymer interactions is outside of the scope of this report. However, we feel that a brief discussion of the observed SPRi results is warranted. The counter-intuitive adsorption of both CN and FN to PAA-c, which should electrostatically repel both CN and FN, suggests the net charge of

(34) Hemmersam, A. G.; Rechendorff, K.; Foss, M.; Sutherland, D. S.; Besenbacher, F. *J. Colloid Interface Sci.* **2008**, *320*(1), 110–116.
(35) Ghiggeri, G. M.; Ginevri, F.; Candiano, G.; Oleggini, R.; Perfumo, F.; Queirolo, C.; Gusmano, R. *Kidney International* **1987**, *32*(4), 547–553.
(36) Laos, K.; Parker, R.; Moffat, J.; Wellner, N.; Ring, S. G. *Carbohydr. Polym.* **2006**, *65*(3), 235–242.
(37) Barbani, N.; Lazzeri, L.; Cristallini, C.; Cascone, M. G.; Polacco, G.; Pizzirani, G. *J. Appl. Polym. Sci.* **1999**, *72*(7), 971–976.
(38) Baujard-Lamotte, L.; Noinville, S.; Goubard, F.; Marque, P.; Pauthe, E. *Colloids Surf., B* **2008**, *63*(1), 129–137.
(39) Wittmer, C. R.; Phelps, J. A.; Saltzman, W. M.; Van Tassel, P. R. *Biomaterials* **2007**, *28*(5), 851–860.
(40) Servagent-Noinville, S.; Revault, M.; Quiquampoix, H.; Baron, M. H. *J. Colloid Interface Sci.* **2000**, *221*(2), 273–283.
(41) Khung, Y. L.; Barritt, G.; Voelcker, N. H. *Exp. Cell Res.* **2008**, *314*(4), 789–800.
(42) Cole, M. A.; Voelcker, N. H.; Thissen, H. *Smart Mater. Struct.* **2007**, *16*, 2222–2228.
(43) Kingshott, P.; Thissen, H.; Griesser, H. J. *Biomaterials* **2002**, *23*(9), 2043–2056.
(44) Stenger, D. A.; Pike, C. J.; Hickman, J. J.; Cotman, C. W. *Brain Res.* **1993**, *630*(1−2), 136–147.
(45) Liu, S.; Vareiro, M.; Fraser, S.; Jenkins, A. T. A. *Langmuir* **2005**, *21*(19), 8572–8575.
(46) Teare, D. O. H.; Emmison, N.; Ton-That, C.; Bradley, R. H. *J. Colloid Interface Sci.* **2001**, *234*(1), 84–89.

Table 1. Association and Dissociation Rates, Binding Constant and Total Binding Capacity of CN type I, FN, and BSA to PAA-c, PEI-c, and PLL-c Obtained by Fitting a First Order Kinetic Process to Kinetic Data Obtained (Supporting Information Figure SI1, Figure SI2, and Figure SI3) by SPRi

	CN type I				FN				BSA			
	k_a (s^{-1} M^{-1}) ($\times 10^3$)	k_d (s^{-1}) ($\times 10^{-4}$)	K (M^{-1}) ($\times 10^6$)	$\Gamma_{s\infty}$ (mg/m^2)	k_a (s^{-1} M^{-1}) ($\times 10^3$)	k_d (s^{-1}) ($\times 10^{-4}$)	K (M^{-1}) ($\times 10^6$)	$\Gamma_{s\infty}$ (mg/m^2)	k_a (s^{-1} M^{-1}) ($\times 10^3$)	k_d (s^{-1}) ($\times 10^{-4}$)	K (M^{-1}) ($\times 10^6$)	$\Gamma_{s\infty}$ (mg/m^2)
PAA	102.40	0.401	2555.5	15.7	69.94	2.55	274.4	15.3	NA	NA	NA	NA
PEI	15.33	2.999	51.1	0.5	35.87	8.67	41.4	3.2	17.38	12.68	13.7	3.8
PLL	8.32	3.546	23.5	0.1	35.81	3.84	93.4	0.5	5.81	4.61	12.6	3.2

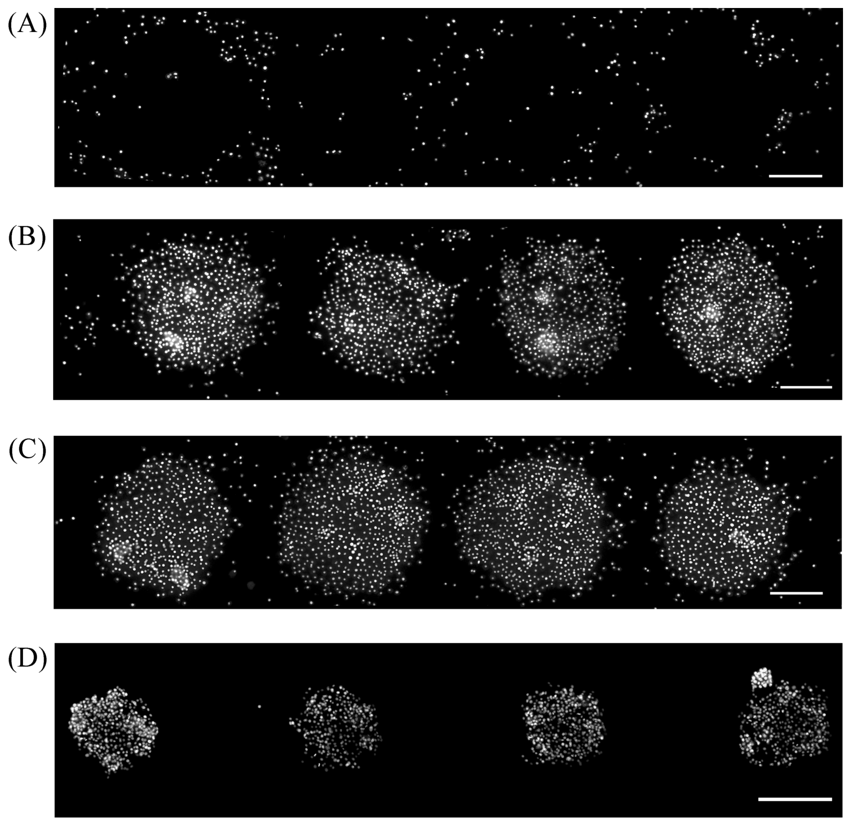

Figure 9. Fluorescence microscopy images of Hoechst 33342 stained SK-N-SH cells grown for 24 h on (A) PAA-c, (B) PEI-c, (C) PLL-c, all printed at 4.0 mg/mL, and (D) PAA-c treated with CN arrayed onto PEG coated surface. Scale bar is 250 μm.

the protein is not dominating its surface adsorption behavior in this case, as opposed to BSA adsorption, which is determined by electrostatics. Comparing the three proteins, CN type I is a protein fibril that at physiological pH has an overall weak negative charge given its pI of 5.5;[37] however with a very high axial ratio, both positively and negatively charged domains are able to be present on the protein's surface, which can undergo binding interactions with the negative charge on the PAA-c polymer.[39,43] The mediation of protein adsorption to a like-charged interface by a single domain on the surface of the protein of opposite charge to the protein's net surface charge has been previously reported.[47,48] Similar considerations apply for FN.[38] The formation of a thicker FN layer on a negatively charged as opposed to a positively charged surface has previously been measured using optical waveguide lightmode spectroscopy.[39] The smaller, globular structure of BSA makes it inflexible to orientations that would minimize the free energy at its surface.[40] Therefore, electrostatic interactions of BSA with a surface a limited to surfaces with an opposite charge to the protein's net charge.

Assessment of Cell Attachment to Polymer Arrays. Further to the SPRi analysis of biomolecular adsorption to a polymer microarray, PAA-c, PEI-c, and PLL-c arrays on the HDI-PEG coated surface were subjected to cell attachment assays. SK-N-SH neuroblastoma cells were seeded onto the polymer array and after 24 h were stained using Hoechst 33342 and observed by fluorescence microscopy. SK-N-SH was used as a model cell line which is adhesive to many different surfaces.[41] Representative images of cells adhering onto microarray spots are shown in Figure 9. PEI-c and PLL-c clearly promoted neuroblastoma cell attachment as determined by the large number of cells aligning with the underlying polymer array as compared with the low cell numbers on the PEG background (Figure 9B,C). PEG is well-known for its ability to resist cell attachment and protein adsorption; thus, low cell attachment on this layer was expected,[42,43] while the presence of amine groups has previously been shown to promote cell attachment, particularly with neuronal cells.[44] Conversely, cell attachment was poor on the PAA-c (Figure 9A). Interestingly, an even lower cell density was observed on these polymer spots as compared with the underlying PEG

(47) Taborelli, M.; Eng, L.; Descouts, P.; Ranieri, J. P.; Bellamkonda, R.; Aebischer, P. *J. Biomed. Mater. Res.* **1995**, *29*(6), 707–714.

(48) Escriou, V.; Ciolina, C.; Helbling-Leclerc, A.; Wils, P.; Scherman, D. *Cell Biol. Toxicol.* **1998**, *14*, 95–104.

coating. The inhibition of cell attachment by PAA has been previously reported for a number of different cell types by electrostatic repulsion with the negative charge on the cell membrane.[46−48]

Comparing cell attachment with the protein adsorption experiments, a clear correlation between cell attachment and BSA adsorption was observed. This may suggest that cell attachment is mediated by the adsorption of negatively charged serum proteins, which has previously been reported.[45] Under normal cell culture conditions in the presence of serum, cell attachment is observed to occur over a period of a few hours; thus, the kinetics of the measured protein adsorption would suggest that protein is able to adsorb to the surface before cells attach.[46] However, in the case of BSA adsorption, which is used to prevent cell attachment,[47] it is unlikely to mediate cell attachment. The correlation between BSA adsorption and cell attachment suggests that both processes occur by the same underlying mechanism, that is, electrostatic interactions. Here, the overall negative charge of the cell membrane[48] will be electrostatically attracted to the positive surface charge of the PEI and PLL spots and likewise be repelled from the negatively charged PAA spots. The preadsorption of negatively charged, cell-adhesive serum proteins may also mediate the cell attachment event.[46] However, determining clear correlations between protein−surface interactions and cell attachment behavior is intrinsically difficult due to the complex nature of cell attachment, which can be influenced by surface properties such as chemistry, inclusion of biological cues, elastic modulus, wettability, charge, and topography as well as cell culture conditions such as the cell line, the concentration of serum, and the time period of incubation.

It is interesting to note that cell attachment did not occur on the PAA-c despite this surface being suitable for the adsorption of ECM proteins while it did occur on PEI-c and PLL-c, which were seen to resist CN type I adsorption (Supporting Information Figure SI1 and Table 1). This result may have implications for long-term cell growth on these surfaces. PEI or PLL coatings may resist the formation of an ECM layer in cell culture, while PAA coatings may, over time, become susceptible to cell attachment by the adsorption of secreted collagen fibrils. Moreover, the inclusion of FN and CN in the cell culture media may also promote cell attachment on the PAA-c. This was investigated by first incubating a PAA-c array with a 50 μg/mL CN solution and then seeding SK-N-SH on this array. PAA-c was chosen for this study, rather than PEI-c or PLL-c, as it typically resisted cell attachment. This pretreatment resulted in cells readily attaching to the PAA-c spots (compare Figure 9A,D), switching these spots from low fouling to cell adhesive.

Conclusion

The label-free characterization of a polymer array containing chemically and morphologically distinct surface features using SPRi has been achieved. A method has been developed whereby changes in reflectivity measured during a typical fixed angle SPR experiment can be related to the corresponding shift in resonance angle. This methodology was first validated by comparing the experimental results of a liquid medium change on a polymer microarray featuring spots of 0−30 nm thickness, giving the results expected from theory. We then utilized this methodology to study the kinetics and thermodynamics of adsorption of CN type I, FN, and BSA to a polymer microarray of positively and negatively charged polymers. For this, a novel approach to producing a low-fouling background for SPR applications was implemented. The SPR chip was first coated with a thin plasma polymer layer that was modified with HDI in order to attach a low-fouling PEG layer. BSA adsorption to the polymer array followed the expected trends assuming electrostatic interactions, however, CN type I and FN, despite having a negative charge at physiological pH, adsorbed on both positively and negatively charged surface chemistries. The end-on adsorption of both these proteins to PAA was suggested based on our data. This result highlighted the complex behavior of biomolecules at surfaces and, thus, the difficulties associated with correlating protein and cellular behavior, and also the potential of high-throughput analysis tools for the study of biointerfacial interactions.

Comparison of protein adsorption studies with cell attachment assays conducted with SK-N-SH in serum over 24 h suggested that cell attachment is largely driven by electrostatic interactions between the cationic surface coatings and the negatively charged cellular membrane, and that it may also be mediated by the preadsorption of negatively charged, cell adhesive serum proteins. Interestingly, the adsorption of ECM proteins such as CN type I to a PAA surface coating enable cell attachment to proceed despite electrostatic repulsion between the carboxyl groups on the PAA and the negatively charged cellular membrane.

The results demonstrate the ability of the label-free technique SPRi to achieve useful kinetic and thermodynamic insights into the biomolecular behavior within a polymer microarray format without the need for advanced fabrication approaches to ensure a homogeneous surface. Use of a larger polymer library would allow for the high-throughput determination of the suitability of particular materials for specific biomedical applications, including tissue engineering, drug delivery, and implant development, and would engender insights into the underlying mechanisms of biomolecular adsorption and cell attachment.

Acknowledgment. Support from Flinders University, the Australian Research Council and CSIRO is kindly acknowledged.

Supporting Information Available: A complete description of the kinetic analysis and associated equations, all kinetic plots for protein adsorption to the polymer array, the summary of the fit of $d\Gamma_s/dt$ against Γ_s for protein adsorption and the calculation of $\Gamma_{side\text{-}on}$ and $\Gamma_{end\text{-}on}$. This material is available free of charge via the Internet at http://pubs.acs.org.